



High-Temperature Oxidation and Corrosion Behaviour of APS CoCrAlY + Cr₃C₂-NiCr Composite Coating

H. S. Nithin¹ · K. M. Nishchitha² · V. Shamanth³ · K. Hemanth³ · K. Anand Babu³

Received: 9 September 2019 / Revised: 20 December 2019 / Accepted: 21 January 2020 / Published online: 30 January 2020
© Springer Nature Switzerland AG 2020

Abstract

An approach of chrome carbide-based composite coating entailing of hard phase (Cr₃C₂-NiCr) and matrix-CoCrAlY was tailored to encounter the severe environments such as elevated temperature oxidation, corrosion and erosion in gas turbine application. CoCrAlY + Cr₃C₂-NiCr coating was deposited by atmospheric plasma spray process. Oxidation and hot corrosion tests were conducted under cyclic conditions in Na₂SO₄-V₂O₅ salt environment at 700 °C. The oxidation and hot corrosion behaviour base metal and coated samples were evaluated by thermogravimetric method. Scanning electron microscopy/energy-dispersive spectroscopy (SEM/EDS) and X-ray diffraction techniques were used to characterize the tested samples in terms of elemental and phase analysis. Microhardness of the composite coating is 318 ± 26 HV and the adhesion strength is found to be 11.5 ± 2.5 MPa. The uncoated alloys exhibited limited weight gain for the initial oxidation cycles followed by linear weight gain curve with the increasing in thermocycles. The CoCrAlY + Cr₃C₂-NiCr coating experienced good corrosion resistance as compared to substrates- MDN 321 and Superni 76 at 700 °C. The coatings subjected to oxidation and hot corrosion showed slow-scale growth kinetics with parabolic rate constant (Kp) value of 0.4 and 0.053 10⁻¹⁰ g² cm⁻⁴ s⁻¹, respectively. The higher Cr content in the coating resulted in the growth of Cr₂O₃ and its spinel CoCr₂O₄ as a strong phase is beneficial for oxidation and corrosion resistance.

Keywords Plasma spray process · Cermet coatings · Hot corrosion kinetics · Chrome-carbide · Oxides/spinel oxides

1 Introduction

Thermal spray coatings are the promising technique to maintain mechanical stability of the components at high temperature by providing protection against severe surface degradation such as high-temperature corrosion, oxidation, erosion and wear [1, 2]. Aero engines, land-based gas turbines and boilers, are the applications experience these degradations. The components of gas turbines will experience degradation at wide range of temperatures. Transition duct and Combustor of gas turbine operate at temperature of nearly 800 °C, whereas turbine vanes, exit blades and discs operate at the

range of 500–600 °C [3, 4]. MCrAlY (M = Ni, Co and CoNi) is a unique coating combination renowned for good oxidation and corrosion resistance at higher temperatures [2]. Nicholls et al. [5] investigated that NiCrAlY provides better corrosion resistance at temperature above 850 °C (Type I) and CoCrAlY coatings are preferable for low-temperature (Type II) hot corrosion condition.

However, MCrAlY coatings are not preferable for tribological applications specifically at high temperature as their lower hardness leads to severe wear under sliding and rotating conditions [6]. Hence, reinforcement of hard phase to MCrAlY coatings is one of the feasible solution to enhance the mechanical properties and to combat against both corrosion and tribological degradation.

WC, CrC, TiC, Al₂O₃, MoS₂, YSZ and so on are the carbides and oxides reinforced to advance the mechanical properties of MCrAlY coatings [7–9]. Chrom carbide with nickel chrom (Cr₃C₂-NiCr) is used for high-temperature wear resistance in various industrial applications. Many studies have been reported on Cr₃C₂-NiCr combination by varying the NiCr (binder) percentage and literature says Cr₃C₂ with

✉ H. S. Nithin
nithinshiv1989@gmail.com; nhs@mcehassan.ac.in

¹ Department of Mechanical Engineering, Malnad College of Engineering, Hassan, India

² Department of Mechanical Engineering, BGSIT, Adichunchanagiri University, Mandya, India

³ School of Mechanical Engineering, REVA University, Bangalore, India

25 wt% of NiCr provides better wear resistance up to 850 °C [10–12]. The binder percentage is increased up to 50% and investigated for corrosion resistance, whereas tribological resistance shows a decremented value [11].

Most of the research articles related to hard phase reinforced composite coatings focused on only phase evolution and tribological properties [7–11]. Many components in gas turbines typically experience concurrent oxidation, hot corrosion, wear degradations at different temperature range, etc [2–4]. There is a need and high interest to assess the performance of hard phase reinforced composite coatings in oxidizing and corrosive environment. Only few studies explain the corrosion behaviour of hard phase reinforced composite coating which is explained below.

Moreover, recent research articles explain carbide-based coatings with composite binder phases, such as $M\text{CrAlY}$ ($M = \text{Co, Ni \& Fe}$) NiCrBSi and NiCrMoNbAl that generally exhibit superior corrosion resistance than traditional binder phases, such as Co, Ni, CoCr and CoCr [12]. The present study focuses on the degradation that occurs at 500–800 °C; hence, the CoCrAlY coating has been selected.

In the present study, CoCrAlY coating reinforced with hard phase $\text{Cr}_3\text{C}_2\text{-NiCr}$ is produced using plasma spray coating technique. The cyclic oxidation and hot corrosion behaviour of CoCrAlY + $\text{Cr}_3\text{C}_2\text{-NiCr}$ composite coating in static air and molten salt ($\text{Na}_2\text{SO}_4\text{-60\%V}_2\text{O}_5$) environment at 700 °C have been examined.

2 Materials and Methods

The austenitic steel (MDN321) and Ni-based superalloy plates (Superni 76) procured from MIDANI, Hyderabad, India, was used as substrate material. The chemical composition of MDN 321 is 0.1C–1.46Mn–0.55Si–18.13Cr–0.62Ti–10.36Ni–Bal Fe and Superni 76 is 21.87Cr–20Fe–9Mo–1.39Co–0.52W–0.44Mn–0.3Si–0.14Ti–0.08C–bal Ni (wt%). The samples were cut into the dimension of 25 × 25 × 3 mm and grit blasted by alumina particles of 150 μm size to produce rough surface. The NiCr coating was used as bond coat on substrate for better adhesion of composite coating. The CoCrAlY powder is reinforced with 30% of agglomerated $\text{Cr}_3\text{C}_2\text{-NiCr}$ to produce a composite feed stock. The chemical composition of CoCrAlY (CC-110) is Co23Cr13Al0.62Y and of CrC25Ni is $\text{Cr}_3\text{C}_2\text{-NiCr}$ (CRC-300-1). All the coating powders are procured from Praxair-India and stated in weight percentage (wt%). CoCrAlY + 30% $\text{Cr}_3\text{C}_2\text{-NiCr}$ composite coating was deposited by plasma spray technique using METCO USA 3 MB equipment and the spray parameters are reported in Table 1. Laser diffraction technique (Cilas 1064, France) was used to measure the nominal particle size distribution of the coating powders as per ASTM C1070 and reported in Table 2. The morphology and

Table 1 Coating condition of plasma spray process

Argon	
Pressure	0.7 MPa
Flow	40 L min ⁻¹
Hydrogen	
Pressure	0.35 MPa
Flow	7 L min ⁻¹
Current	490 A
Voltage	60 V
Powder feed	60 g min ⁻¹
Stand of distance	100–125 mm

Table 2 Particles size (μm) distribution of coating powders

Particle size	CoCrAlY + $\text{Cr}_3\text{C}_2\text{-NiCr}$
D (0.1)	19.35
D (0.5)	48.62
D (0.9)	89.30
Mean	51.42

distribution of powder are shown in Fig. 1a. The presence of agglomerated Cr_3C_2 particle is shown in energy-dispersive spectroscopy (EDS) analysis (Fig. 1b).

The hardness was measured using Omni-tech Vickers micro-indenter (MVH-S-AUTO) under 300 g loads and a dwell time of 10 s. The indentations were taken along the coating cross-section of the coating and the indentations were done at 20 random points within the coating to obtain the average hardness (HV) value.

Cyclic oxidation and hot corrosion tests were conducted at 700 °C in static air and hot corrosion in molten salt environment as referred in the previous research article [13]. The change in weight occurred after each cycle was recorded to understand the oxidation and corrosion kinetics. X-ray diffractometer (XRD, with $\text{CuK}\alpha$ radiation) and scanning electron microscope [Scanning electron microscopy (SEM), JOEL-JSM-6380LA] were utilized to identify the phases and morphology of coating powder, as-coated, oxidized and corroded coatings.

3 Results

3.1 Morphology of the Structure

Coating is produced by depositing layers of melted/partially melted splats on substrate resulted in thin, elongated and dense lamellar structure. Series of splats layers are deposited to obtain required coating thickness. Bond coat is applied between topcoat to substrate for the purpose of good adhesion and it is shown in Fig. 2. The average coating thickness

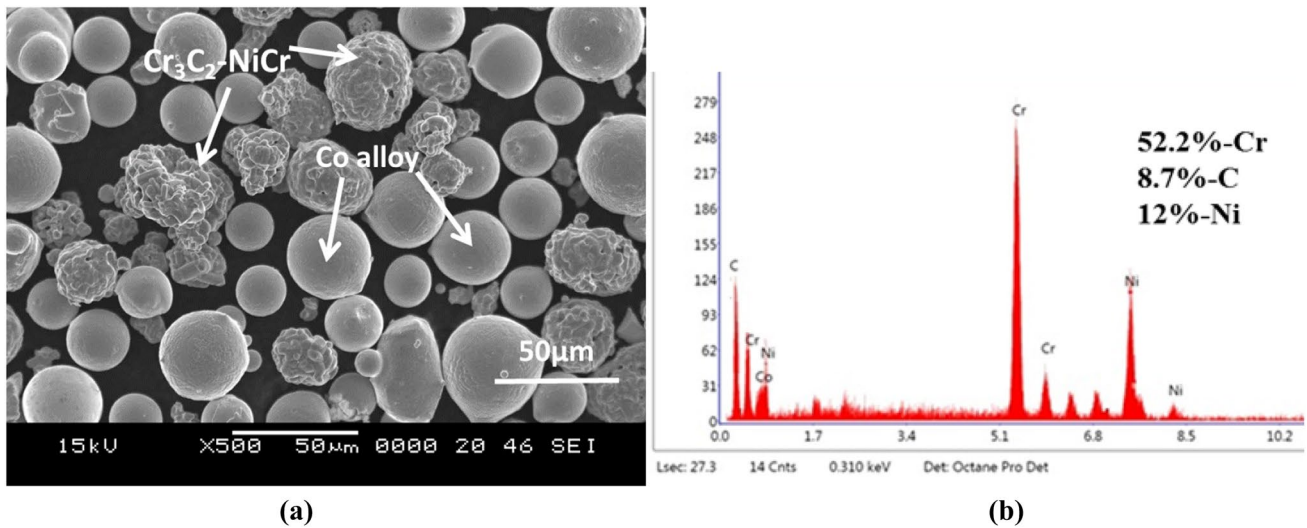


Fig. 1 Morphology of CoCrAlY + Cr₃C₂-NiCr powder

Fig. 2 Morphology of a CoCrAlY + Cr₃C₂-NiCr coating at the cross-section and b magnified image

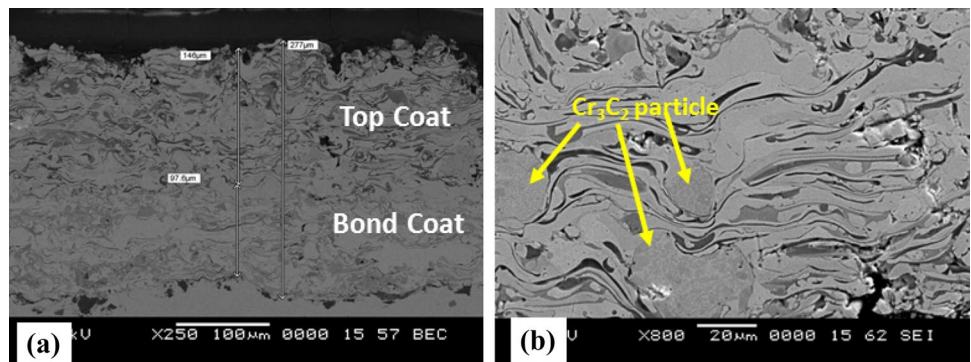


Table 3 Vickers microhardness value

Material	Average hardness (HV)
MDN 321	198
Superni 76	212
Coating	318

was measured by taking SEM image along the cross-section and it is observed as 265 µm, which includes the top coat of 135–140 µm. Distribution of Cr₃C₂-NiCr particles with the Co matrix is shown in Fig. 2b. No cracks are observed along the coating–substrate interface, which results in good adhesion between substrate and coating. The average microhardness of the coating is 318 ± 26 HV, and Table 3 shows the hardness value of substrate and bond coat.

Bond strength of coating is evaluated as per ASTM-C633-13 standard and the top coat should be less than 300 µm. Better adhesion of the coating is expected for lesser

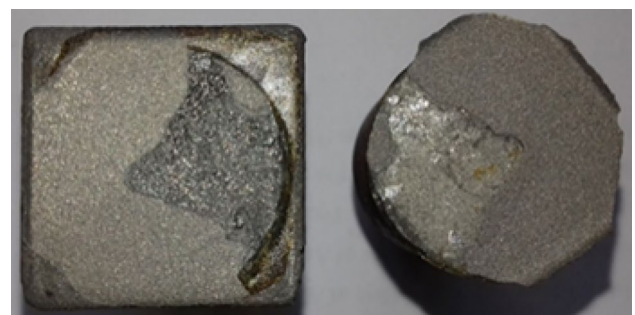


Fig. 3 Fractured surface of adhesion test coating

thickness as the effect of internal stress will be lower for smaller thickness. Figure 3 shows the typical fracture occurring between coating and the substrate indicating the adhesive failure, which implies that cohesion strength between splats is good. The adhesion strengths of CoCrAlY + Cr₃C₂-NiCr coatings are found to be 11.5 ± 2.5 MPa, respectively.

3.2 Phase Analysis

XRD patterns of CoCrAlY + Cr₃C₂-NiCr powder and as-coated sample are shown in Fig. 4. Co, Cr and α -Al₂O₃ are the major peaks observed in as-coated pattern of both coatings. The Al in the coating composition undergoes oxidation and forms Al₂O₃ due to longer inflight time of spray process. Whereas intermediate peaks are indexed to Cr₃C₂ carbides (00-001-1186) and Al₅Co₂ (00-048-1302). The decarburization of carbide particles due to high-temperature exposure of coatings particle during the coating process resulted in the existence of Cr₇C₃ (00-036-1482) phases in the as-coated XRD pattern [14].

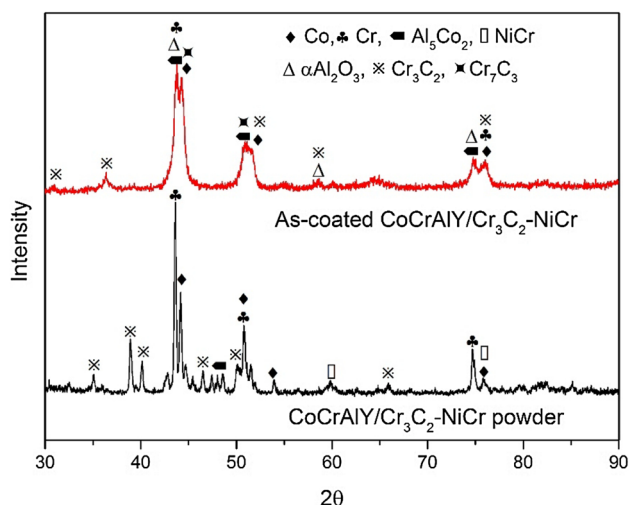


Fig. 4 XRD patterns of CoCrAlY + Cr₃C₂-NiCr powder and as-sprayed coating

3.3 Thermo Cyclic Oxidation and Scale Formation

The oxidation kinetics of coated and uncoated alloys is estimated by plotting weight change against number of cycles as shown in Fig. 5. The weight change of oxidized sample is normalized to its unit area (Fig. 5a) and squared to evaluate the oxidation kinetics (Fig. 5b). Uncoated alloys experience parabolic weight gain (slow growth rate) during the initial cycles and incremental weight gain is observed after some cycles which continues throughout the oxidation cycles in lower rate. The overall weight gain of MDN 321 and Superni 76 is observed to be 1.8 and 1.2 mg cm⁻², respectively. The overall weight gain of oxidized CoCrAlY + Cr₃C₂-NiCr-coated MDN 321 and Superni 76 alloys is 2.97 and 3.20 mg cm⁻², respectively. Significant weight gain is observed in the initial oxidation cycles and as the oxidation cycles continue, linear weight gain nature is witnessed. Linear least-square algorithm method is used to calculate the parabolic rate constant (Kp), i.e. in the form of $(dW/A)^2 = Kp \times t$, where dW/A is weight gain per unit area and t is time in seconds. 0.44 and 0.38 10⁻¹⁰ g² cm⁻⁴ s⁻¹ are Kp values of coated MDN 321 and coated Superni 76, respectively (Fig. 5b).

X-ray diffraction patterns of oxidized CoCrAlY + Cr₃C₂-NiCr-coated alloys at 700 °C are listed in Fig. 6. Both coated alloys show similar phases of compounds, oxides and spinel oxides. Major peaks in the patterns indexed to Cr₂O₃ and CoO, while Cr₂O₃ is indexed to two of the major and many minor peaks indicating the major constituent in the protective oxide scale. Intermediate peak indexed to α -Al₂O₃, Al₅Co₂, CoCr₂O₄ and NiCr₂O₄.

The surface and cross-section morphology of oxidized coatings are shown in Fig. 7. The surface oxide scale in

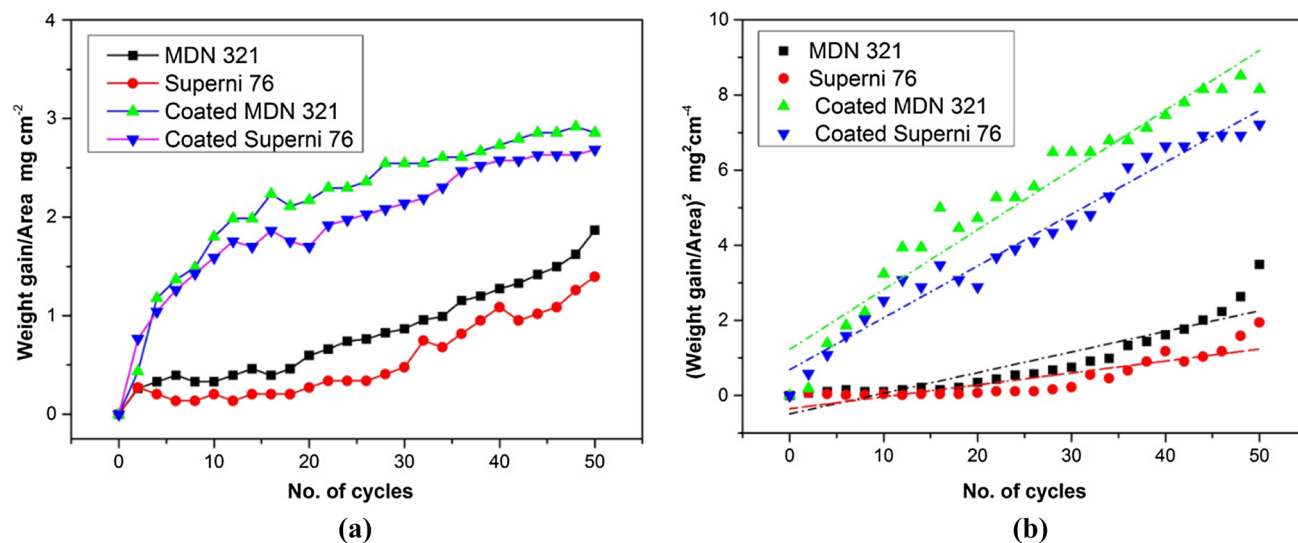


Fig. 5 Oxidation cycle plots **a** weight gain per unit area, **b** square of weight gain per unit area

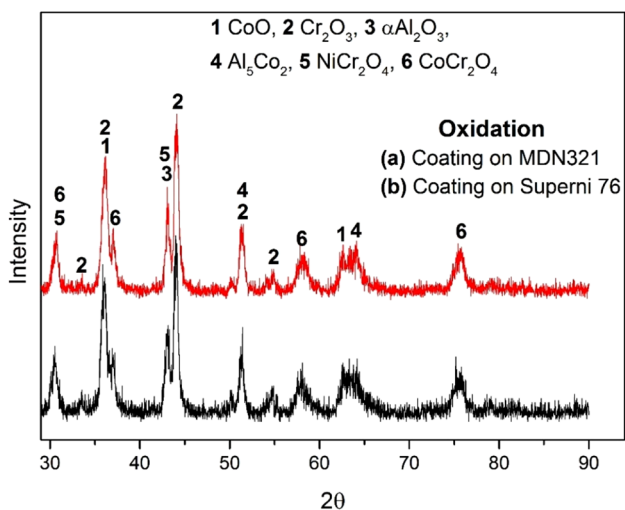


Fig. 6 XRD patterns of oxidized coatings at 700 °C

Fig. 7a and b illustrates the existence of combination of globular structure and patches of least oxidized splats. Also, the oxidation occurred along the splat boundaries of least oxidized splat appeared as web-like structure (Fig. 7a).

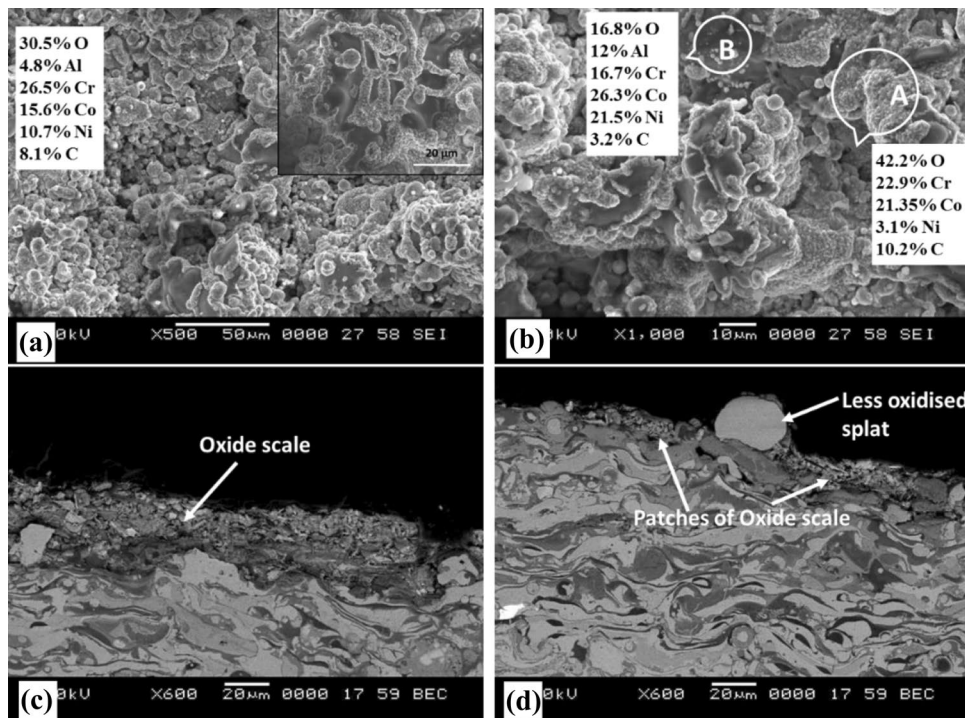
The EDS analysis exposed the presence Co, Cr, Ni and O rich content in globular structure infers the occurrence of oxides of Co, Cr, Ni and its spinels. The smooth splat-like structure (Fig. 7a) shows the presence of minimum O with rich Co, Cr and Ni which may expose the presence of CoCr and NiCr compound. The presence of Cr₂O₃

(01-076-0147), CoO (00-001-1227), CoCr₂O₄ (00-024-0326) and NiCr₂O₄ on the surface is evident from the XRD analysis of oxidized samples (Fig. 6).

The thickness of oxide layer is measured along the cross-section (Fig. 7c, d) and observed as 10–20 μm. Discontinuous oxide layer is observed throughout the surface with patches of least oxidized splat structure is appeared in the oxide scale. The presence of thin discontinuous oxide-rich content on the outermost surface is apparent from X-ray mapping (Fig. 8). The X-ray mapping shows the distribution of Co, Cr, Ni and Al in the oxide-rich surface. As the oxidation time proceeds, the nucleation of CoO–Cr₂O₃ and NiO–Cr₂O₃ on the coating surface resulted in spinel oxides- CoCr₂O₄ and NiCr₂O₄. The presence of oxides and spinel oxides on the surface would restrict the oxygen entry deep inside the coating and reduces the oxidation and scaling rate. Also coating with lower oxide layer thickness plays a major role in reducing the chances of delamination. Cr being one of the highest coating element in the composition resulted in the formation of Cr₂O₃ phase provides greater resistance to oxidation.

From the above discussion, it can be inferred that the oxidized CoCrAlY + Cr₃C₂-NiCr coating is the combination of continuous globular structure and patches of least oxidized splats. The uncoated alloys experienced lower weight gain than coated alloys during the initial cycles, and they expressed the gradual weight gain in each cycle throughout the oxidation cycles. This shows that the ability

Fig. 7 Oxidized coating on a, b surface morphology and EDS analysis, c cross-section



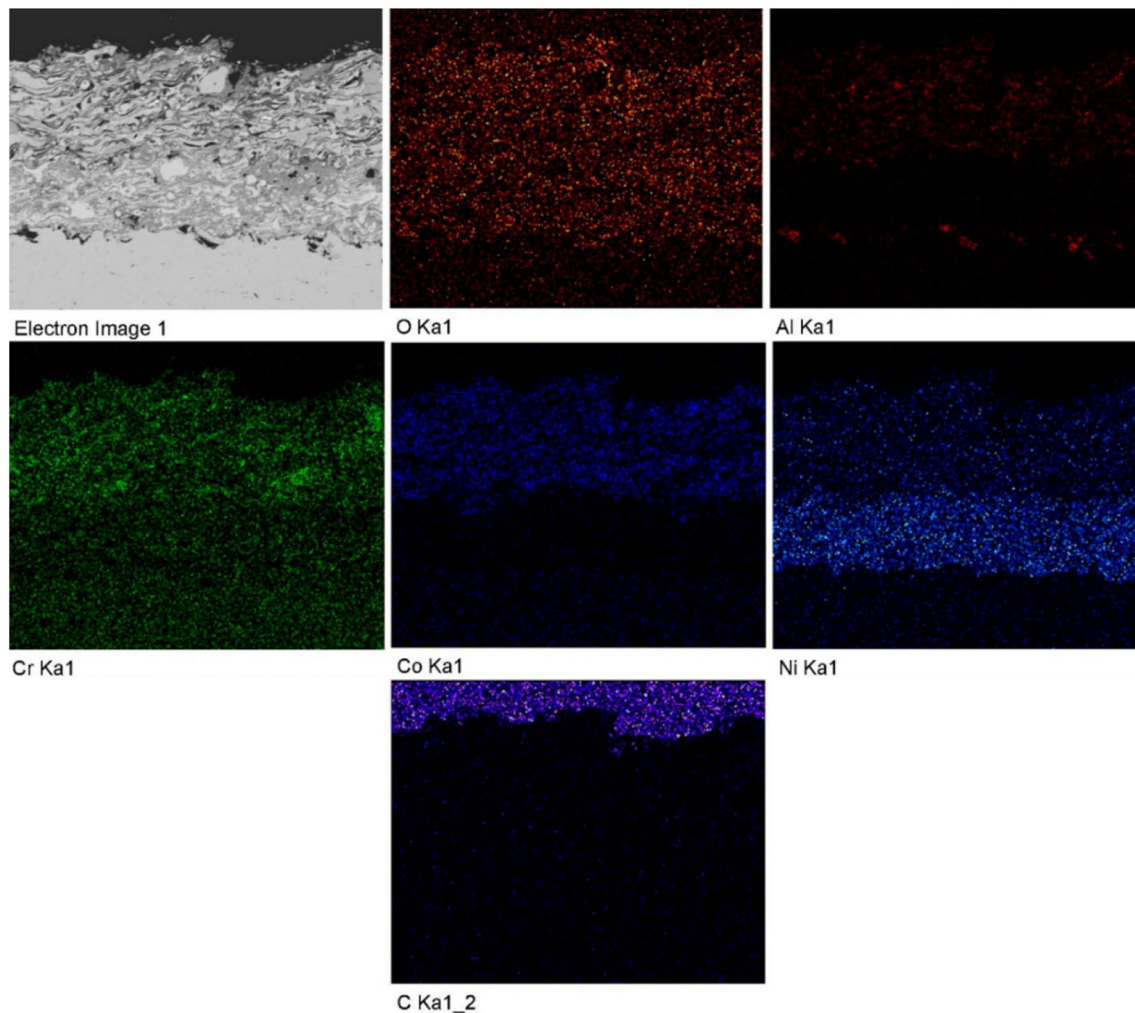


Fig. 8 Elemental analysis along the cross-section of oxidized coating

of surface oxides on uncoated alloys would protect against oxidation to the limited extent.

3.4 Thermocyclic Hot Corrosion Kinetics and Scale

The weight gain (mg cm^{-2}) plots of uncoated alloys and CoCrAlY + Cr_3C_2 -NiCr coatings as a function of time expressed in number of cycles are shown in Fig. 9. MDN 321 alloy shows higher weight gain than Superni 76 with overall weight gain of about 9.5 and 7.8 mg cm^{-2} , respectively. The overall weight gain after 50 cycles of corroded CoCrAlY + Cr_3C_2 -NiCr-coated MDN 321 and Superni 76 alloys is 1.73 and 1.66 mg cm^{-2} , respectively. Higher weight gain is observed in the initial stages where oxidation is predominant and the steady-state weight gain is observed with subsequent corrosion cycles. After few cycles, the steady-state weight gain is achieved till the completion of 50 cycles which is mainly due to the development of stable protective oxide layer. The weight gain square data plotted against time

to determine the corrosion kinetics is shown in Fig. 9. The parabolic rate constant (K_p) value of coated MDN 321 and Superni 76 alloys is 0.053 and $0.048 \cdot 10^{-10} \text{ g}^2 \text{ cm}^{-4} \text{ s}^{-1}$, respectively. The present coating shows better hot corrosion resistance by least weight gain than CoCrAlY + Al_2O_3 , CoCrAlY + CeO_2 and CoCrAlY + WC-Co coatings as resulted in the references [15, 16].

XRD patterns of coated alloys subjected to hot corrosion at 700°C are shown in Fig. 10. The major peaks in coated alloys are indexed to CoO and Cr_2O_3 whereas the intermediate/minor peaks indexed to $\alpha\text{-Al}_2\text{O}_3$, V_2O_5 , CoAl_2O_4 , CoCr_2O_4 and NiCr_2O_4 . The presence of NiCr as binder in Cr_3C_2 is responsible for the formation of NiCr_2O_4 spinel oxide during the corrosion cycles. The peaks and phases obtained on both the coated alloys after subjected to corrosion are similar.

The surface morphology of corroded coating is shown in Fig. 11. Surface oxide is developed due to the oxidation of each splats and it has appeared as a continuous closely

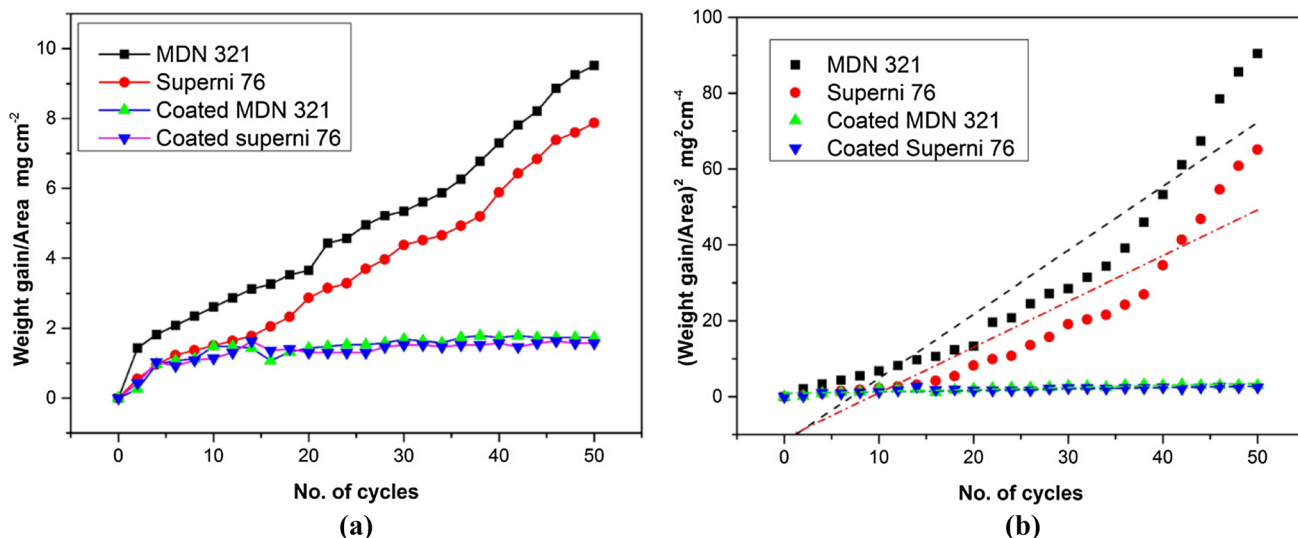


Fig. 9 Graph of hot corrosion cycles a weight gain per unit area, b square of weight gain per unit area

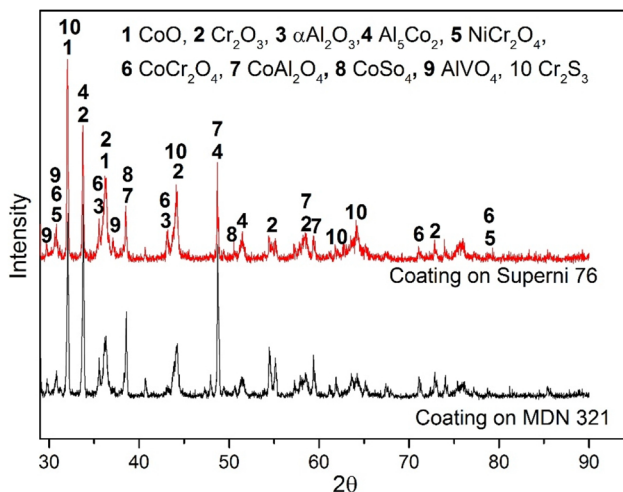


Fig. 10 XRD patterns for coatings subjected to hot corrosion at 700 °C

packed globular structure. This structure is observed throughout the coating surface after subjecting to hot corrosion. EDS analysis of point ‘A’ and ‘C’ in Fig. 11a and b shows the dominant presence of oxides of Co, Cr and Al, indicating the occurrence of probable phases CoO , Cr_2O_3 , Al_2O_3 and the combination of these oxide as CoCr_2O_4 and CoAl_2O_4 spinels. The point ‘B’ has appreciable composition of many major elements such as O, Co, Cr, Ni and V leading to the interpretation of presence of NiCr_2O_4 and $\text{V}_2\text{O}_5/\text{CrV}_2\text{O}_4$. Thus, the oxide scale developed on the coating surface may be the combination of CoO , Cr_2O_3 , Al_2O_3 and spinels such as CoCr_2O_4 , CoAl_2O_4 and NiCr_2O_4 . The presence of these phases is also confirmed by the XRD results (Fig. 10). Figure 11c and d shows the formation of a thin

oxide scale on the upper most layer of the coating surface and lamellar structure of the coating is retained below the oxide scale. This shows that the developed surface oxide scale has protected the underneath coating and more importantly the substrate alloys. The oxide layer thickness is mentioned in Table 4 as observed in Fig. 11c. The elemental composition at various point of the oxidized coating cross-section is analysed by EDS analysis (Fig. 11c, d) and reported in Table 5. The O percentage at point ‘1’ is higher and is gradually reduced as we move to point ‘4’ showing that the oxide scale acts as barrier for the corrosion species to enter into the coating.

X-ray mapping (Fig. 12) of coating cross-section shows the distribution of Co, Cr Ni and O throughout the coating cross-section, whereas the O distribution is denser at the coating surface indicating the presence of oxides of Co, Cr, Ni, Al and its spinels. The presence of Al is observed in the top coat and also at the interface of bond coat and substrate which is due to the embedment of alumina particles during grit blasting prior to the coating process. Also, the distribution of V and Na salts is observed only at the surface of the coating and these salts can be interpreted as the oxide layer acting as a blockade to the entry of salts. The presence of these oxides and eutectic salts is supported by surface EDS and is strongly supported by XRD analysis (Fig. 10).

4 Discussion

The weight gain of the $\text{CoCrAlY} + \text{Cr}_3\text{C}_2\text{-NiCr}$ -coated alloys are found to be 82% and 79% lesser as compared to uncoated MDN 321 and Superni 76 substrates, respectively. The hot corrosion resistance of $\text{CoCrAlY} + \text{Cr}_3\text{C}_2\text{-NiCr}$ is

Fig. 11 Surface morphology (a, b) and cross-section (c, d) images of hot corroded coating

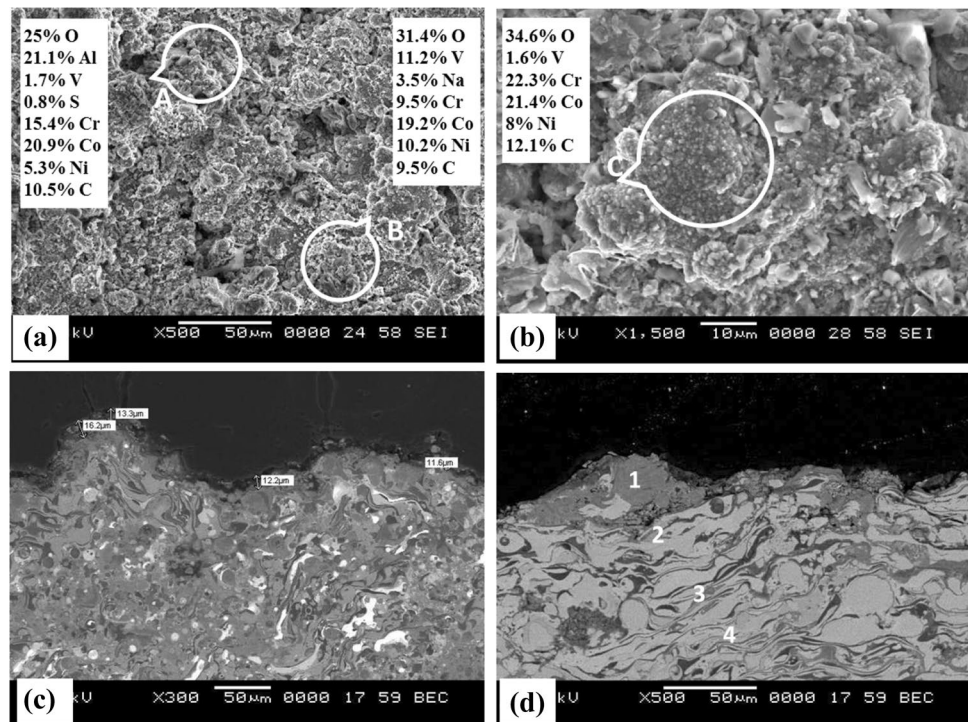


Table 4 Thickness of top coat, bond coat and oxide layer

Sl. no	Particulars	Thickness (μm)
1	Top coat	140–150
2	Bond coat	95–105
3	Oxide layer	10–16

Table 5 Point EDS of CoCrAlY + Cr₃C₂-NiCr coating cross-section in wt%

Elements	Region 1	Region 2	Region 3	Region 4
O	27.2	12.9	2.8	2.1
Na	0.2	–	–	–
V	0.9	–	–	–
Al	7	6.8	22.6	9.4
Cr	19.4	27.1	15.8	22.8
Co	22.4	23.6	32.6	32.1
Ni	20.8	24.4	19.4	15.8
C	2.1	4.8	1	2.8

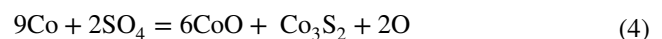
attributed to the nature of protective oxide scale developed on the surface.

The low-temperature hot corrosion (Type II) occurs more often at the range of 650 to 800 °C in molten corrosive salt. In such conditions, salts react with metal and metal oxides, which leads to the formation of eutectic

sulphates having lower melting point such as Co–Co₄S₃ (880 °C), Ni–Ni₃S₂ (635 °C), Na₂SO₄–NiSO₄ (671 °C), Na₂SO₄–CoSO₄ (575 °C), NaVO₃ (630 °C) and CoSO₄ (735 °C) [17]. During the initial stage of hot corrosion, active elements of coating Co, Cr and Al oxidized to form CoO, Cr₂O₃ and Al₂O₃. The metal ions utilize atmospheric oxygen ion and oxygen ion present in Na₂SO₄–V₂O₅ salt. The probable chemical reactions to form metal oxides are shown in equations.



In other case, the molten SO₄ would diffuse into the coating and react with Co being a major coating element oxidized to CoO by utilizing oxide ion present in the salt (Eq. 4)



The loss of oxygen ion in the salt increases the activity of sodium, sulphur and vanadium salt resulted in the acidic fluxing of metal oxides. Fluxing of metal/metal oxides leads to the formation of eutectics such as CoSO₄, Cr₂S₃ and AlVO₄. These eutectics will promote the corrosion rate more aggressively when it reaches the molten salt. The probable reaction during the growth of these eutectics is shown in Eqs. (5 and 6).

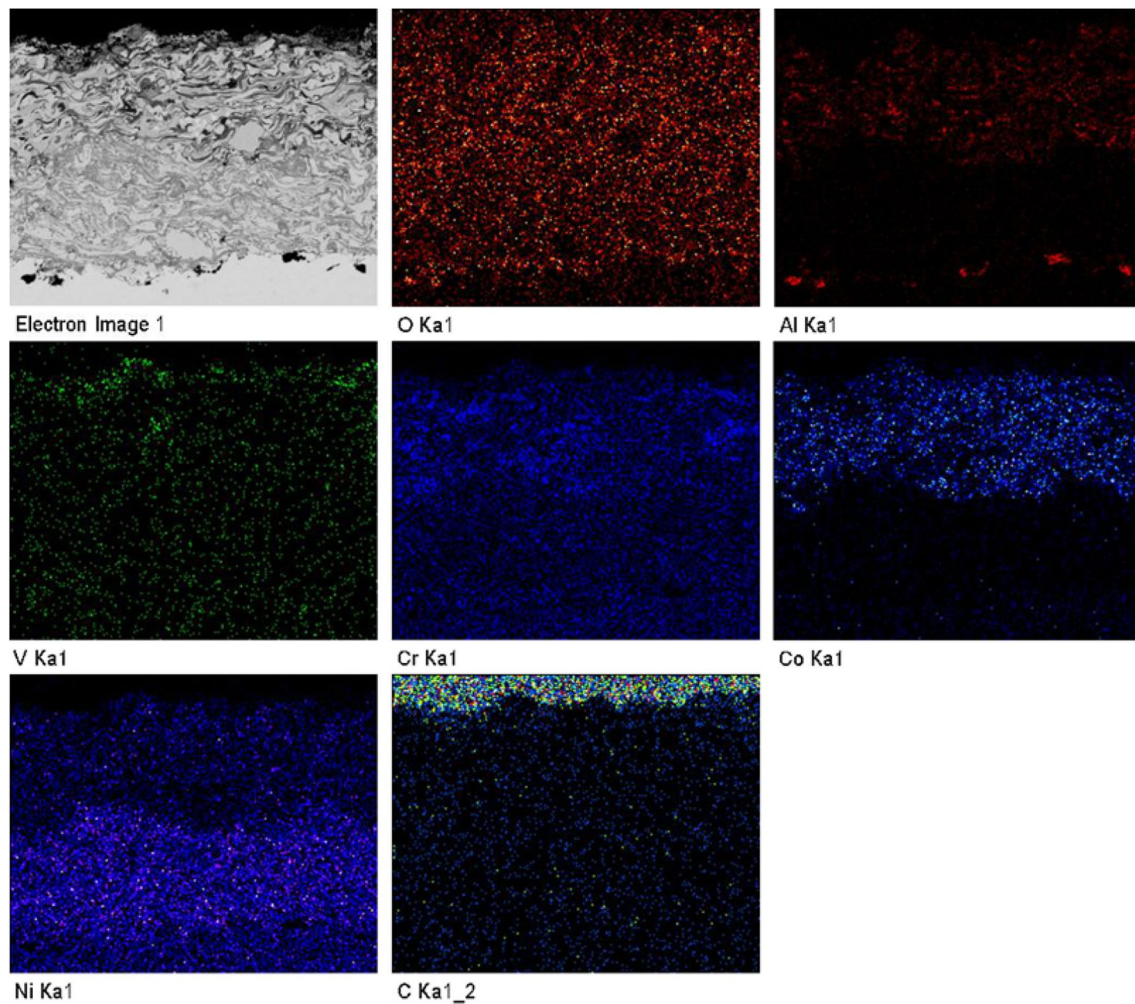
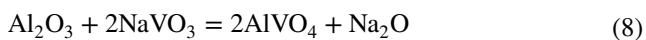


Fig. 12 X-ray mapping of oxidized coating along the cross-section



The probable chemical reactions for the growth of AlVO_4 are shown in Eq. 7. The fluxing action of NaVO_3 with Al_2O_3 due to lower melting point (Eq. 8).



During the initial stage of hot corrosion, CoO dissolution is predominant; further, salt is saturated in CoO resulting in the formation of CoSO_4 sulphate (Eq. 5). Cr combined with highly active sulphur leads to the growth of Cr_2S_3 . These CoSO_4 and Cr_2S_3 eutectics have melting point of 735°C and 1350°C , respectively, which are higher than the corrosion test temperature. Hence, these eutectics are more

stable and thereby providing the resistance to corrosion degradation. Evidently, CoSO_4 and Cr_2S_3 are observed in the XRD analysis. The eutectics $\text{Ni-Ni}_3\text{S}_2$, $\text{Na}_2\text{SO}_4\text{-NiSO}_4$ and $\text{Na}_2\text{SO}_4\text{-CoSO}_4$ having lower melting point undergo fluxing action with protective metal oxides resulting in the higher weight gain rate at the initial cycles.

Also Nicholls et al. [5] recommended that the Cr in MCrAlY coating is suggested to be up to 40% for better hot corrosion resistance. $\text{CoCrAlY} + \text{Cr}_3\text{C}_2\text{-NiCr}$ coating contains 36 wt% of Cr including the Cr present in the reinforcement ($\text{Cr}_3\text{C}_2\text{-NiCr}$) which is substantially higher and close to higher limit. This leads to the preferential oxidation of Cr at the early stage of corrosion to form Cr_2O_3 as a major oxide. Cr_2O_3 provides resistance against oxidation and corrosion by restricting the inward diffusion of oxygen below the temperatures of 800°C . Above 800°C , the Cr_2O_3 starts to evaporate and form volatile chromium oxide (CrO_3) which is not beneficial to resist oxidation [13]. As the corrosion cycle progresses, nucleation of CoO and Cr_2O_3 to form CoCr_2O_4 spinel oxide

(Eq. 9) with subsequent hot corrosion cycles is also one of the major phase observed in XRD analysis [18]. The presence of small amount of Ni in Cr_3C_2 -NiCr reinforcement oxidized to NiO and nucleation of NiO and Cr_2O_3 results in the formation of NiCr_2O_4 (Eq. 10). The spinel oxides NiCr_2O_4 have also been identified by the XRD analysis. NiCr_2O_4 and CoCr_2O_4 are protective oxides that could limit the outward diffusion of Co, thus slowing down the corrosion rate.



Chatterjee et al. [19] also observed that spinel usually has lower diffusion coefficients of cations and anions, which is beneficial for reducing the oxidation rate. The presence of stronger Cr_2O_3 and CoO with spinel oxides and stable eutectics helps to provide a barrier to the entry of corrosive species. The oxidation and corrosion mechanism of coating elements are expressed in the form of chemical reaction in the previous article [19]. The thin (8–15 μm) oxide scale is also beneficial since it undergoes less thermal stress during cyclic loading and it has better adhesion with the coating surface. These oxides act as blockade to the diffusion of oxygen and corrosive species of molten salt inside of coating; hence, coating region beneath the oxide scale remains unoxidized. Corrosion products are confined to the outermost oxide scale. Few researchers reported that the presence of CoCr_2O_4 and NiCr_2O_4 spinels on the plasma-sprayed corroded CoNiCrAlY/ Cr_2O_3 coating surface has improved resistance against oxidizing environment [20–22].

Different oxide mixtures developed during the high-temperature exposure, such as CoO, Cr_2O_3 , CoCr_2O_4 , NiCr_2O_4 and stable eutectic CoSO_4 , Cr_2S_3 , will bestow the properties of the coating in restricting the corrosion degradation. However, strong Cr_2O_3 and stable eutectics CoSO_4 , Cr_2S_3 plays a major role for restricting the corrosion. The oxidation resistance of the uncoated alloys is limited to few thermocycles and showed linear weight gain curve with the increasing in thermocycles, which explicit the limitation of uncoated alloys. At the early cycles of oxidation and corrosion coating shows higher weight gain due to oxidation of active elements and filling up pores present at splat boundaries by oxide scale. Once the stable oxides are developed on the surface, parabolic weight gain nature will be appeared. The coated alloys have experienced better corrosion resistance than uncoated alloys by stable protective oxides and spinel oxides.

5 Conclusion

Co-based coatings reinforced with Cr_3C_2 -NiCr were deposited by plasma spray technique. The coating formed by deposition of layers of melted/partially melted splats and hard phase Cr_3C_2 -NiCr is uniformly distributed in the coating matrix. Both in oxidation and in hot corrosion conditions, the uncoated alloys exhibited linear weight gain curve, while coatings show parabolic weight gain nature. The presence of continuously packed globular structure is observed throughout the coating surface in both oxidized and corroded condition. Also, oxide scales formed on the surface are free from interfacial spallation and superficial cracks which in turn act as a diffusion blockade to the entry of corrosion species. The presence of high Cr content in the coating is sufficient to the growth of Cr_2O_3 as a strong phase is highly beneficial for corrosion resistance which is supported by stable CoSO_4 , Cr_2C_3 eutectics and CoCr_2O_4 , NiCr_2O_4 spinel oxides.

Compliance with Ethical Standards

Conflict of interest On behalf of all authors, the corresponding author states that there is no conflict of interest.

References

1. Lu J, Zhu S, Wang F (2011) High temperature corrosion behavior of an AIP NiCoCrAlY coating modified by aluminizing. *Surf Coat Technol* 205:5053–5058
2. James AW, Rajagopalan S (2014) Gas turbines: operating conditions, components and material requirements. In: Shirzadi A, Jackson S (eds) *Structural alloys for power plants*. Woodhead Publishing, Cambridge, pp 3–21
3. Miller BA (1986) *Failure analysis and prevention*. ASM Metals Handbook, USA
4. Baiamonte L, Marra F, Gazzola S, Giovanetto P, Bartuli C, Valente T, Pulci G (2016) Thermal sprayed coatings for hot corrosion protection of exhaust valves in naval diesel engines. *Surf Coat Technol* 295:78–87
5. Nicholls JR, Simms NJ, Chan WY, Evans HE (2002) Smart overlay coatings—concept and practice. *Surf Coat Technol* 149(2–3):236–244
6. Cabral-Miramontes JA, Gaona-Tiburcio C, Almeraya-Calderón F, Estupiñan-Lopez FH, Pedraza-Basulto GK, Poblano-Salas CA (2014) Parameter studies on high-velocity oxy-fuel spraying of CoNiCrAlY coatings used in the aeronautical industry. *Int J Corros*. <https://doi.org/10.1155/2014/703806>
7. Ramesh MR, Prakash S, Nath SK, Sapra PK, Venkataraman B (2010) Solid particle erosion of HVOF sprayed WC-Co/NiCr-FeSiB coatings. *Wear* 269(3–4):197–205
8. Kim K, Korsunsky AM (2010) Dissipated energy and fretting damage in CoCrAlY-MoS₂ coatings. *Tribol Int* 43(3):676–684
9. Nithin HS, Desai V, Ramesh MR (2018) Elevated temperature solid particle erosion behaviour of carbide reinforced CoCrAlY composite coatings. *Mater Res Express* 5(6):066529

10. Matthews S, Berger LM (2016) Long-term compositional/microstructural development of Cr_3C_2 -NiCr coatings at 500 °C, 700 °C and 900 °C. *Int J Refract Metal Hard Mater* 59:1–8
11. Murthy JK, Venkataraman B (2006) Abrasive wear behaviour of WC-CoCr and Cr_3C_2 -20 (NiCr) deposited by HVOF and detonation spray processes. *Surf Coat Technol* 200(8):2642–2652
12. Zhou W, Zhou K, Deng C, Zeng K, Li Y (2017) Hot corrosion behavior of HVOF-sprayed Cr_3C_2 -WC-NiCoCrMo coating. *Ceram Int* 43(12):9390–9400
13. Seo D, Ogawa K, Suzuki Y, Ichimura K, Shoji T, Murata S (2008) Comparative study on oxidation behavior of selected MCrAlY coatings by elemental concentration profile analysis. *Appl Surf Sci* 255(5):2581–2590
14. Zhou W, Zhou K, Deng C, Zeng K, Li Y (2017) Hot corrosion behaviour of HVOF-sprayed Cr_3C_2 -NiCrMoNbAl coating. *Surf Coat Technol* 309:849–859
15. Nithin HS, Vijay D, Ramesh MR (2018) Cyclic oxidation and Hot Corrosion behavior of plasma-sprayed CoCrAlY+ WC-Co coating on turbine alloys. *J Fail Anal Prev* 18(5):1133–1142
16. Chatha SS, Sidhu HS, Sidhu BS (2012) High temperature hot corrosion behaviour of NiCr and Cr_3C_2 -NiCr coatings on T91 boiler steel in an aggressive environment at 750 °C. *Surf Coat Technol* 206(19–20):3839–3850
17. Fan QX, Jiang SM, Yu HJ, Gong J, Sun C (2014) Microstructure and hot corrosion behaviors of two Co modified aluminide coatings on a Ni-based superalloy at 700 °C. *Appl Surf Sci* 311:214–223
18. Ramesh MR, Prakash S, Nath SK, Sapra PK, Krishnamurthy N (2011) Evaluation of thermocyclic oxidation behavior of HVOF-sprayed NiCrFeSiB coatings on boiler tube steels. *J Therm Spray Technol* 20(5):992–1000
19. Chatterjee UK, Bose SK, Roy SK (2001) Environmental degradation of metals: corrosion technology series, vol 14. CRC Press, Boca Raton
20. Yuan K, Peng RL, Li XH, Johansson S, Wang YD (2015) Some aspects of elemental behaviour in HVOF MCrAlY coatings in high-temperature oxidation. *Surf Coat Technol* 261:86–101
21. Zhang T, Huang C, Lan H, Du L, Zhang W (2016) Oxidation and hot corrosion behavior of plasma-sprayed MCrAlY-Cr₂O₃ coatings. *J Therm Spray Technol* 25(6):1208–1216
22. Hidalgo VH, Varela FB, Menéndez AC, Martínez SP (2001) A comparative study of high-temperature erosion wear of plasma-sprayed NiCrBSiFe and WC-NiCrBSiFe coatings under simulated coal-fired boiler conditions. *Tribol Int* 34(3):161–169

Publisher's Note Springer Nature remains neutral with regard to jurisdictional claims in published maps and institutional affiliations.